Available online at www.sciencedirect.com

ScienceDirect

Procedia Manufacturing 48 (2020) 498–507

Procedia MANUFACTURING

www.elsevier.com/locate/procedia

48th SME North American Manufacturing Research Conference, NAMRC 48 (Cancelled due to COVID-19)

Effect of Workpiece Curvature on Axial Surface Error Profile in Flat End-Milling of Thin-walled Components

Ankit Agarwal, K. A. Desai*

Department of Mechanical Engineering, Indian Institute of Technology Jodhpur, Jodhpur – 342037, Rajasthan, India

Abstract

The advancements in the domain of CAD/CAM and CNC machine tools facilitated machining of complex geometric shapes to meet functional requirements and/or aesthetic appearances. These shapes combine several geometric features such as zero curvature (straight), constant curvature (circular) and variable curvature surfaces. The components often contain thin-walled sections having inherently lower stiffness that induces static deflections transforming into surface error and violation of error limits specified by the designer. This paper presents a comparison of deflection induced surface error profile generated during the end milling of zero and constant curvature thin-walled components. The proposed framework incorporates computational model to estimate cutting forces, Finite Element Analysis (FEA) model to compute workpiece deflections, and surface generation mechanism to derive error profile. The paper also investigates the effect of change in the radial engagement area due to workpiece curvature by introducing the concept of '*Equivalent Radial Depth of Cut*'. Further, the effect of change in workpiece curvature is investigated on the surface error profile in the paper. The proposed framework has been generalized to accommodate the variation of workpiece geometry, and the results are validated by conducting a set of end milling experiments.

Keywords: End Milling; Thin-wall components; Curved surfaces; Static deflections; Surface error

1. Introduction

A large variety of components in automotive, energy, and shipbuilding industries involve thin-walled sections containing complex geometric shapes, e.g. honeycomb structures, spars and ribs, avionic trays, etc. These components amalgamate planar and curved sections to meet complex functional and aesthetic requirements. The advancements in Computer-Aided Design and Manufacturing (CAD/CAM) and extensive use of CNC machine tools in the manufacturing activity lead to machining processes replacing metalworking and assembly operations to fabricate these components. The end milling operation involving flat and/or ball end mills is preferred due to its capability to manufacture such components in a variety of materials with better accuracy and productivity. The flat end mills are employed for roughing to remove large amounts of material from the forged or cast blocks followed by finishing operation performed using ball end mills. The roughing operation is similar to 2.5D pocket machining with contour parallel tool paths, and it is performed at elevated cutting conditions to achieve higher productivity. The tool path encompasses straight and/or convex/concave circular segments combined to obtain desired contour geometry. The component rigidity reduces considerably with the progress of machining resulting in increased static deflections of the component. As component rigidity is least during the final pass of roughing, static deflections leave considerable uncut material or roughing surface error to be removed during the finishing pass. It is necessary to estimate this surface error accurately as it will help in the effective design of the finishing operation. It has been reported in the literature that the variation of surface error during machining of low rigidity or thin-walled components is dependent on the workpiece geometry [1]. The thin-walled components with curved surfaces exhibit significantly different characteristics compared to planar or straight components. The curved geometries can be machined from a concave or convex side, also referred to as synclastic and anticlastic machining, respectively, in the literature. The present study aims to investigate the effect of workpiece geometry on nature and amount of surface error generated during the final roughing pass of thin-walled components.

* Corresponding author. Tel.: +91-291 280 1509 .
E-mail address: kadesai@iitj.ac.in (K. A. Desai).

10.1016/j.promfg.2020.05.074

The milling of thin-walled straight and curved components has been actively studied and reported in the literature. These studies primarily deal with modeling of cutting forces, estimation of machining attributes such as tool-workpiece deflections, prediction and control of surface error, etc. Sabberwal and Koenigsberger [2] introduced Mechanistic force model by correlating cutting forces with the uncut chip area. The prediction capability of the model was enhanced by introducing cutter runout [3] and replacing average chip thickness with instantaneous chip thickness [4]. The model was extended subsequently to circular geometries by introducing workpiece radius in the mathematical formulations determining process geometry parameters i.e. uncut chip thickness and engagement angle [5, 6]. The process geometry were modified further for variable curvature surfaces [7] and cutter runout [8, 9]. The Mechanistic force model can predict cutting forces with reasonable accuracy over a wide range of cutting conditions, and the same is adopted in the present study.

The literature also present attempts considering estimation and compensation of surface error during milling of straight and circular geometries. The studies considering estimation of surface error in transient situations e.g., machining at corners of the rectangular pocket are also reported [10, 11]. The variation of surface error during milling of thin-walled plates was studied considering tool and workpiece deflections [12]. The Finite Element Analysis (FEA) based approach was also suggested to predict [13] and compensate [14] static deflection induced surface errors during machining of thin-walled components. Rao and Rao [15] analyzed the effect of curvature on tool-workpiece engagement conditions to predict tool deflection induced surface errors. Dépincé and Hascoët [16] proposed a tool path compensation technique to minimize tool deflection induced surface errors. Schmitz et al. [17] examined the effect of cutter runout on surface error and stability during milling of curved geometries. Bera et al. [1] estimated tool-workpiece deflections to analyze the variation of surface error during milling of thin-walled tubular geometries. It was shown that the deflections of tubular geometries are significantly lesser due to increased stiffness of the component. The study was extended further by developing compensation scheme to minimize the surface error [18]. The influence of cutting widths on axial variation of surface error was investigated by Desai and Rao [19] in the presence of tool deflections followed by development of methodology to regulate the error variation for curved geometries [20]. The FEA based methodology has also been explored to examine the effect of cutting temperature [21] and cutting widths [22] on surface error due to deflection of workpiece. Wimmer et al. [23] examined the influence of cutter diameter, number of flutes and helix angle on surface error during milling of thin-walled components. Recently, an optimisation algorithm was presented to plan material removal in series of blocks to control workpiece deformations [24]. Li and Zhu [25] applied tool path optimisation algorithm to minimize surface error during 5-axis milling of thin-walled parts.

Based on the review of literature, it can be concluded that estimation and compensation of surface error during end-milling operation for different geometries have been studied thoroughly as an independent entity. There has been no study that compares surface error variation for different geometries. Additionally, the studies do not investigate the influence of engagement area and chip load on surface error owing to change of the workpiece geometry. The present study aims to estimate workpiece deflection for different geometries and compares the variation in the magnitude and shape of surface error profile while migrating from zero curvature to constant curvature geometries. Further, the study also investigates the effect of various attributes of curved components such as change in the radius of curvature, variation in engagement area and chip load while machining from convex and concave side. The effect of workpiece rigidity during roughing of thin-walled component is an important parameter that has also been addressed in this study. This is done systematically by keeping other structural parameters and machining conditions unchanged for straight, circular concave and convex geometries.

2. Modeling of Surface Error

The prediction of surface error during end milling of thin-walled components necessitates the development of several computational elements. These elements include Mechanistic force model, workpiece deflection model and surface generation mechanism to transform deflections into surface error. The Mechanistic force model has been adopted in this study to predict cutting forces for both straight and curved components. The workpiece deflections due to cutting forces are estimated using FEA based methodology. The deflections are transformed subsequently into surface error profile for straight and circular components using surface generation mechanism. The following sub-sections summarizes the above-mentioned steps for estimation of surface error.

2.1. Modeling of Cutting Forces

The Mechanistic force model simulates end milling operation by discretizing an end mill into numerous disk elements (n) of equal thickness (dz) along the axial direction. The model estimates cutting forces acting on the cutter in the Feed (F_F) and Normal (F_N) direction corresponding to each engaged flute (k) of the axial disk element (j) at an incremental rotation of the cutter (i) using Eqs. 1-3. The total cutting force $F_s^T(\phi_i)$ ($s = F, N$) a given cutter rotation angle (ϕ_i) is obtained by integrating forces acting on individual disk element for each flute engaged at a discrete cutter rotation (ϕ_i) angle using Eq. 4.

$$\begin{bmatrix} F_F(i,j,k) \\ F_N(i,j,k) \end{bmatrix} = dz\, t_c(i,j,k) \begin{bmatrix} cos\,\beta(i,j,k) & -sin\,\beta(i,j,k) \\ sin\,\beta(i,j,k) & cos\,\beta(i,j,k) \end{bmatrix} \begin{bmatrix} K_T(i,j,k) \\ K_R(i,j,k) \end{bmatrix} \quad (1)$$

$$t_c(i,j,k) = f_{pt}\ sin\,\beta(i,j,k) \quad (2)$$

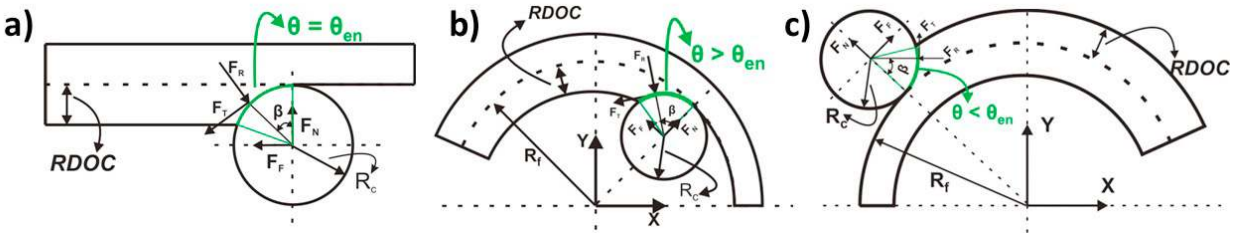

Fig. 1. Schematic Representation for End Milling of Different Geometry: (a) Straight; (b) Concave; (c) Convex

$$\beta(i,j,k) = \phi_i + (k-1)\,\phi_p + \left((j-1)\,dz + \frac{dz}{2}\right)\frac{tan\,(\theta_h)}{R_c} \quad (3)$$

$$F_s^T(\phi_i) = \sum_{i,j,k} F_s(i,j,k) \qquad s = F,N \quad (4)$$

In Eq. 1 $t_c(i,j,k)$ and $\beta(i,j,k)$ represent instantaneous uncut chip thickness and angular position corresponding to j^{th} disc element and k^{th} flute at a cutter rotation angle ϕ_i. The uncut chip thickness $t_c(i,j,k)$ can be expressed geometrically using Eq. 2 as a function of feed per tooth (f_{pt}). The angular position $\beta(i,j,k)$ can be determined using Eq. 3, where ϕ_p, θ_h, R_c represents pitch angle, helix angle and radius of the cutter respectively.

The paper considers machining of straight, concave and convex thin-walled components, which differs in cutting configurations as depicted in Fig. 1. The circular geometry has a constant radius of curvature in comparison to straight geometries having no curvature. Therefore, a generic cutting force model incorporating the effect of variation in workpiece geometry is used in the present study. The f_{pt} for circular components is not same as the actual or programmed feed per tooth (f_a) and depends upon the category of workpiece curvature (concave or convex) and magnitude of the radius of curvature. Similarly, the engagement angle (θ_{en}) also differs with geometry of the workpiece due to change in the dimension of transition area as depicted in Fig. 1. The mathematical formulations for f_{pt} and θ_{en} during machining of straight, concave and convex feature are given in table 1. Here, R_f represents final radius of curvature of workpiece; *RDOC* and *ADOC* represents *Radial and Axial Depth of Cut*.

Table 1. Process Parameters for Straight and Circular Components

	Feed per tooth (f_{pt})	Engagement Angle (θ_{en})
Straight	f_a	$cos^{-1}\left(1 - \frac{RDOC}{R_c}\right)$
Concave	$f_a\left(\frac{R_f - RDOC}{R_f - R_c}\right)$	$cos^{-1}\left(\frac{R_c^2 + (R_f - R_c)^2 - (R_f - RDOC)^2}{2R_c(R_f - R_c)}\right)$
Convex	$f_a\left(\frac{R_f + RDOC}{R_f + R_c}\right)$	$cos^{-1}\left(\frac{R_c^2 + (R_f + R_c)^2 - (R_f + RDOC)^2}{2R_c(R_f + R_c)}\right)$

The terms $K_q(i,j,k)$ $(q = T,R)$, in Eq. 1 are known as Mechanistic cutting constants, and it correlates instantaneous uncut chip thickness with cutting forces. These constants are determined by performing end milling experiments under specific conditions for a given combination of tool and workpiece material. The non-linear relationship between cutting constant $K_q(i,j,k)$ $(q = T,R)$ and instantaneous uncut chip thickness $t_c(i,j,k)$ is derived subsequently using curve fitting (Eq. 5).

$$K_q(i,j,k) = a_q\, e^{-b_q\, t_c(i,j,k)} + c_q \qquad (q = T,R) \quad (5)$$

2.2. Finite Element Modeling

The static deflections of straight and circular thin-walled components are predicted in the present study using Finite Element Analysis (FEA) based methodology due to ease of its integration with the Mechanistic force model. The present study employs MATLAB® and ANSYS Parametric Design Language (APDL) in an integrated manner to predict cutting forces and static deflections of thin-walled components. The thin-walled plates have been modeled as Free-Free-Free-Constrained (FFFC) arrangement i.e. plates are allowed to deflect freely along three sides and constrained at the bottom as shown in Fig. 2. Once the component is modeled and boundary conditions are applied, it is meshed with 3-Dimensional 8-node Solid Shell element (SOLSH 190) with three translational degrees of freedom per node to ensure advantages of using solid elements and its ability to avoid shear locking. The transition zone between tool and workpiece at any instant is labeled as ABCD in Fig. 2 for different geometries. It can be observed that the transition zone is significantly larger in concave side milling for the same *RDOC* and *ADOC*, while it is smaller in convex side milling in comparison to the straight geometry of the same dimensions. The flute enters the transition zone at vertex D along an entry edge DA during milling operation. The helical flute traverses over the transition zone and it is represented using a slant line inclined at an angle θ_h (Fig. 2(b)). The flute exits from the transition zone along exit edge CB and gets completely out of cut at vertex B.

The cutting forces predicted for required geometry using the Mechanistic force model outlined in the previous section are

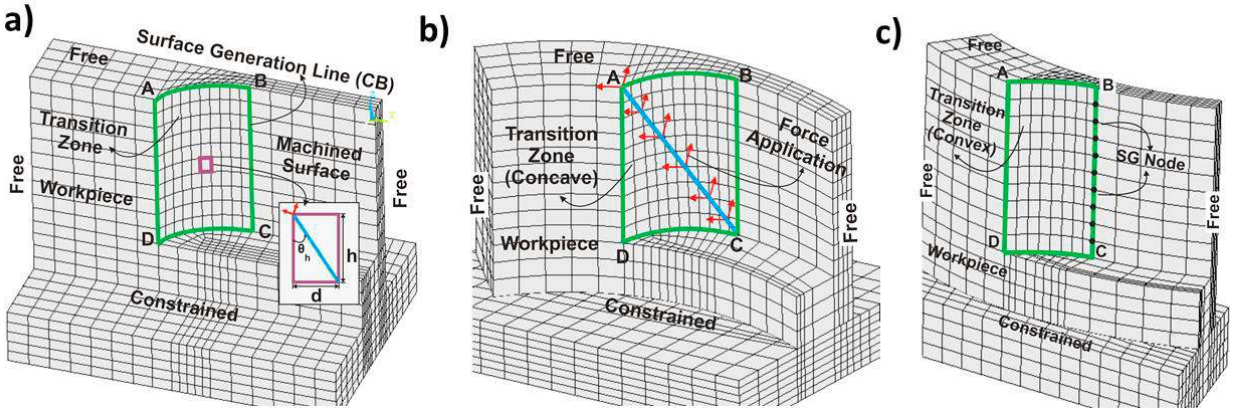

Fig. 2. Workpiece Deflection Modeling. (a) Straight; (b) Concave; (c) Convex

applied along the slant line as depicted in Fig. 2(b). In order to synchronize the direct transfer of elemental cutting force to nodes on the deflection model, the dimensions of quad elements in the transition zone is chosen such that the aspect ratio is equal to $tan\ \theta_h$ as shown in Fig. 2(a). The height (h) of the quad element is equal to the thickness of the disk element (dz) in cutting force model. The area mesh generated in this manner is swept further along the thickness of plate. The transition region is finely meshed in comparison to other portions of the plate as it is of greater interest in predicting static deflections. The cutting forces computed for each disc element are applied on corresponding top-left corner node of the quad element as shown in Fig. 2(a & b). After application of cutting forces at corresponding node in the FE model, the deflections in the normal direction are computed at the surface generation (SG) nodes as shown in Fig. 2(c). These steps are repeated for each incremental rotation of cutter until it traverses the transition zone completely and machined surface is generated. Although the proposed approach is complex and computationally intensive, it mimics actual milling operation appropriately and yields accurate results.

A '*moving*' coordinate system in the form of a local Cartesian coordinate has been used in the FEA of circular components to apply cutting forces and computation of deflection values. The Global cylindrical coordinate system is defined for this purpose at the center of the circular component. The cutting forces are applied in the tangential and normal direction as computed from the cutting force model. The subsequent analysis has been done to obtain deflections in the normal direction. In case of FE analysis of straight components, the application of local coordinate system is not essential as it coincides with the Global coordinate system. An important point to note here is that the deflection in the normal direction to the workpiece surface contributes to surface error; therefore, the deflection in tangential and axial direction is neglected.

2.3. Surface Generation Mechanism

The static deflections of workpiece at the instant of surface generation are reflected in the form of surface error. It is necessary to transform static deflections of thin-walled components into surface error. The machined surface is generated during milling operation when cutting flute passes through the exit edge CB, which is termed as surface generation line and nodes lying on it are termed as surface generation (SG) nodes as shown in Fig. 2(c). Owing to the presence of helix angle along the flute, the surface is generated gradually as the cutter exits the transition zone.

The surface generation commences from the SG node lying at point C and terminates when cutter traverses the SG node lying at point B. The elemental cutting forces from Mechanistic force model are applied to FE model of the workpiece corresponding to the location of helical flute and nodal deflection at SG point is stored as surface error along with its axial coordinate. In the subsequent stage, the cutter is rotated such that SG point slides by amount equal to thickness of disc elements in the force model. The elemental cutting forces corresponding to the new location of flute are computed and applied to the FE model for determination of workpiece deflection and surface error. This process is repeated until surface error at each SG point is computed to derive the complete surface error profile. Therefore at a particular instant of cutter rotation, deflection of each SG node is not important and deflection corresponding to exit node needs to be recorded to estimate the surface error profile.

Figure 3 shows schematic representation of the methodology determining surface error profile during end milling of thin-walled components. The overall computation procedure can be divided into three stages. The first stage comprises integration of Mechanistic force model with APDL and generation of FE model for the component as per the input conditions. The subsequent stage deals with meshing of the component, application of elemental forces and determination of workpiece deflections. The final stage deals with transformation of workpiece deflections into surface error at SG points. An automated program

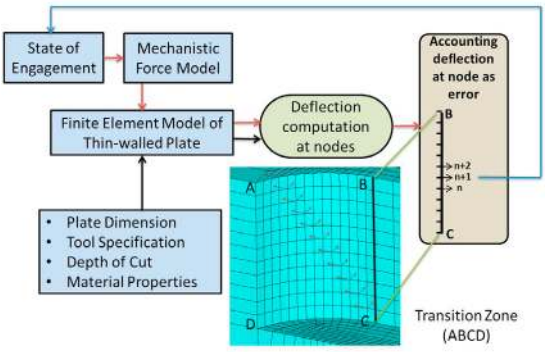

Fig. 3. Methodology for Surface Generation Mechanism

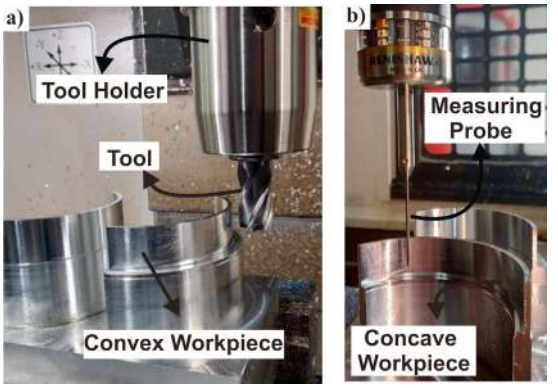

Fig. 4. Experimental Setup: (a) Machining Setup; (b) Measurement Setup

has been developed in this study to determine static deflections of workpiece using FE at each SG node and derive the axial surface error profile.

3. Results and Discussion

The FEA model and surface generation mechanism outlined in the previous section has been applied to predict surface error profile and study characteristics related to milling of straight and circular thin-walled geometries. Section 3.2 compares surface error variation during end milling of straight, circular concave and convex geometries keeping other machining attributes identical. It has been observed that the engagement area varies considerably during end milling of different geometries even though other machining conditions are identical. The concept of '*Equivalent RDOC*' has been devised and presented in section 3.3 to obtain identical engagement area for each geometry. Section 3.4 examines the engagement pattern of cutting flutes with the change of workpiece curvature. Table 2 summarizes workpiece material with relevant properties and cutting tool specifications. The experiments were conducted using 3-axis CNC vertical milling machine and a spindle mounted inspection probe (Renishaw OMP-400) as depicted in Fig. 4.

Table 2. Tool-Workpiece Attributes.

Tool Specification (Kennametal : 4CH1600DK022A)			Workpiece Properties (Aluminium 6061-T6)	
Cutter Diameter	Helix Angle	Number of Flutes	Young's Modulus	Poisson's Ratio
16 mm	30°	4	68.9 GPa	0.33

3.1. Prediction of Cutting Forces

The effectiveness of the Mechanistic force model is examined by performing end milling experiment for straight components. Figure 5 depicts the comparison of cutting forces predicted using computational model and experimentally measured values corresponding to cutting condition listed in Table 3. It can be observed that the cutting forces predicted through Mechanistic model are in good agreement with experimentally measured values. Subsequently, the model has been extended for estimation of cutting forces during milling of circular components using formulations listed in Table 1.

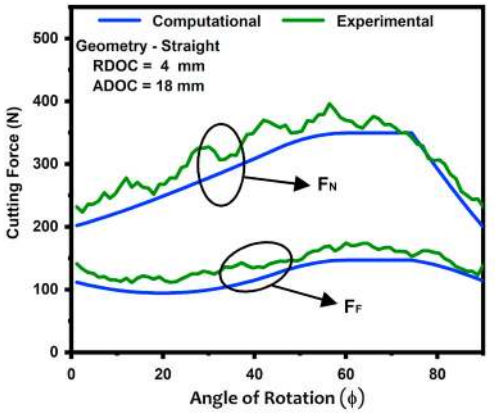

Fig. 5. Comparison of Measured and Predicted Cutting Forces

3.2. Effect of Workpiece Geometry

The curved geometry can be machined from two sides; concave and convex. It has been shown in the previous section that the engagement area or transition zone changes significantly when the component is machined from either of these sides under the same cutting conditions. The concave side engages more while convex side engages less in comparison to straight geometries for the identical cutting conditions. The larger engagement area indicates more material being removed for the same *RDOC* for concave geometries implying higher cutting

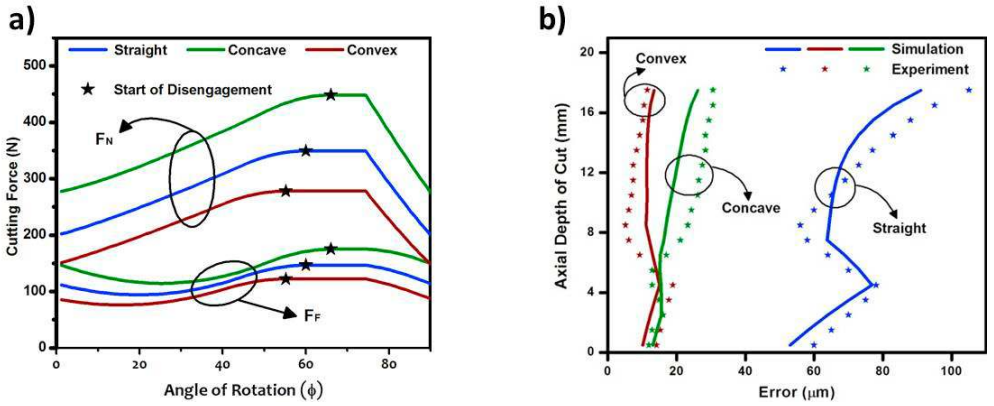

Fig. 6. End Milling of Different Geometry: (a) Cutting Force profile; (b) Surface Error profile

forces. The converse behavior is expected for convex geometries. This section analyzes surface error profile for three different configurations of thin-walled geometries; straight, circular concave and convex with identical process parameters. The workpiece dimensions, cutting conditions for different geometries and other process parameters are summarized in Table 3.

Table 3. Workpiece Dimension and Cutting Condition.

Geometry	Inner Radius (mm)	Outer Radius (mm)	Engagement Angle (θ_{en})
Straight	NA	NA	60°
Concave	35	41	66.77°
Convex	39	45	55.86°

RDOC (mm)	:	4
ADOC (mm)	:	18
Workpiece Dimension (mm)	:	100 x 50 x 6 (L x H x D)
Final Thickness (mm)	:	2
Feed Rate (mm/min)	:	300
Spindle Speed (RPM)	:	2000

Figure 6(a) represents the cutting force variation obtained computationally for three geometries at cutting condition listed in Table 3. The cutting force are higher for concave and lower for convex geometry in comparison to straight components owing to change of the engagement angle as discussed earlier. The variation in engagement angle also varies the start and end of disengagement for all three geometries. Figure 6(b) represents the axial variation of surface error computed computationally and experimentally for three geometries under consideration in the study. It can be observed that the straight components deflect significantly higher in comparison to circular concave and convex components. Although the concave component experiences significantly larger engagement area, chip load and cutting force in comparison to straight geometry, the surface error is quite less. Such behavior can be attributed to the geometric configuration of curved structure which is inherently stiffer in comparison to straight geometries that results into smaller deflection values and thereby surface error. This is a favorable situation for the process planner as it permits use of productive cutting conditions while machining concave geometries. An important point to note here is the magnitude of surface error in concave and convex case is comparable to each other even though the convex geometry experiences much lesser engagement area, chip load and cutting forces in comparison to concave geometry. It is expected that the surface error in case of concave geometry would be much higher than convex counterpart but the same is not observed. The effect of engagement area has been studied in the subsequent subsection in order to investigate this aspect in a greater detail.

3.3. Analysis of Constant Engagement Area

The different configurations of thin-walled components were machined with similar cutting conditions but the engagement area was considerably varying due to different nature of workpiece geometry. In order to investigate this aspect further, the concept of '*Equivalent RDOC*' has been devised by considering constant engagement area in this subsection. The '*Equivalent RDOC*' represents the value at which radial engagement angle is identical for both straight and circular geometries. Figure 8 depicts the schematic representation to understand the concept of '*Equivalent RDOC*'. Figure 8 shows machining with variable *RDOC* for different geometries but the engagement angle is maintained at the same level in each case. The programmed *RDOC* in each case is different due to curved nature of workpiece i.e. concave and convex workpiece curvature. This *RDOC* value is termed as '*Equivalent RDOC*' which offers an identical radial engagement angle for all three geometries. The '*Equivalent RDOC*' can be determined as follows:

- The engagement angle is determined in case of straight geometries for the given *RDOC* and *ADOC* values.

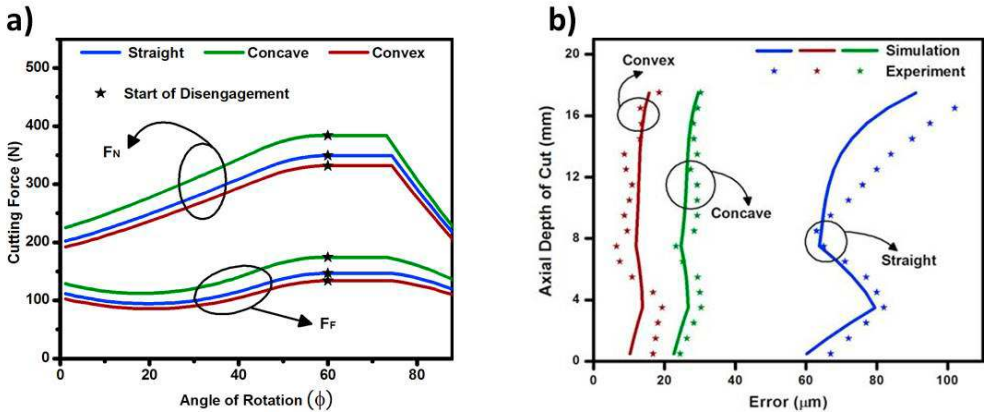

Fig. 7. End Milling of Different Geometry with "*Equivalent RDOC*": (a) Cutting Force profile; (b) Surface Error profile

- The engagement angle for straight geometry is maintained in case of circular convex and concave geometries by varying *RDOC* value.

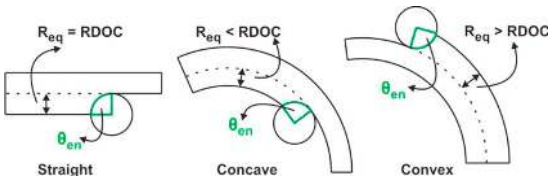

Fig. 8. Constant Engagement Machining with " *Equivalent RDOC*"

The numerical values of '*Equivalent RDOC*' for different geometries are summarized in Table 4. The convex geometry is having larger *RDOC* while concave geometry has smaller *RDOC* than the straight ones. These values are considered as '*Equivalent RDOC*' since it offers constant engagement angle in the each case. In order to implement this concept, initial or un-machined thickness (*D*) of the plate is required to be varied to have the uniformity in the final or machined thickness of the component. This necessitates reduction in the un-machined thickness (*D*) for concave geometry which results into diminishing of workpiece rigidity. Similarly, the un-machined thickness (*D*) increases in case of convex geometry leading to enhanced rigidity for un-machined components. Such variation of initial workpiece rigidity due to different *RDOC* affects the deflection pattern and surface error for the machined component. Table 4 summarizes the cutting conditions and resultant dimensions of the un-machined workpiece for different geometries.

Figure 7(a) represents the cutting force variation obtained computationally for three geometries at cutting conditions listed in Table 4. The cutting force are higher for concave and lower for convex geometry in comparison to straight components. However, the starting instant of disengagement remains identical due to constant angle of engagement for all three geometries. Figure 7(b) shows the comparison of surface error profile obtained computationally and experimentally for

Table 4. Workpiece Dimension and Cutting Condition for '*Equivalent RDOC*'.

Geometry	Inner Radius (mm)	Outer Radius (mm)	Workpiece Dimension (L x H x D)	Equivalent *RDOC* (R_{eq}) (mm)
Straight	NA	NA	100 x 50 x 6	4
Concave	35	41	100 x 50 x 5.32	3.32
Convex	39	45	100 x 50 x 6.53	4.53

ADOC (mm)	:	18
Engagement Angle (θ_{en})	:	60°
Final Thickness (mm)	:	2
Feed Rate (mm/min)	:	300
Spindle Speed (RPM)	:	2000

straight, circular concave and convex geometries. It can be seen that the straight geometry deflects more in comparison to circular geometries owing to lesser stiffness and result into higher surface error. Both, concave and convex geometries deflect significantly lesser than the straight geometry resulting into lower surface error. Also, the convex geometry deflect lesser in comparison to concave geometries. The smaller value of surface error for convex geometries can be attributed to enhanced rigidity of the component which thereby reduces the workpiece deflections. Similarly, concave geometries deflect more and results in to higher surface error due to reduction in the rigidity of the component. It can also be inferred that increase of cutting forces due to higher *RDOC* value in case of convex geometries does not have significant effect on the workpiece deflections and surface error. Based on results shown in Fig. 7, it can be concluded that convex geometries present inherent machining advantage for process planners. These geometries can be machined with elevated cutting conditions and thereby resulting into more productive rough milling operation.

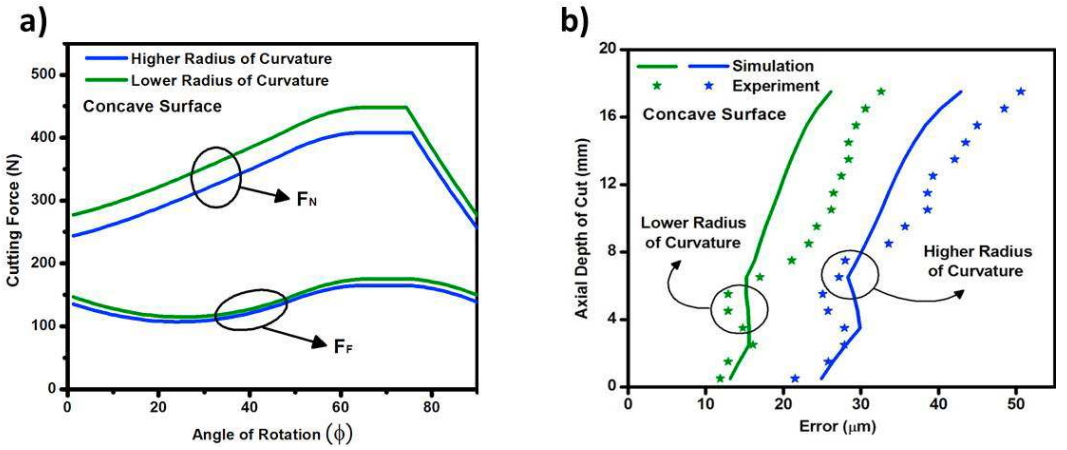

Fig. 9. End Milling of Concave Surface with varying Radius of Curvature: (a) Cutting Force Profile; (b) Surface Error Profile

3.4. *Effect of Workpiece Radius of Curvature*

The present study also analyzes the effect of workpiece curvature on surface error during machining of thin-walled components. To substantiate this aspect, the dimensions of thin-walled component are designed such that the volume of material resisting cutting forces is maintained at constant level as of section 3.2. This has been achieved by maintaining thickness, height and length of component at the same level with variation of workpiece radius. It results into thin-walled components with different workpiece curvature but constant volume of material to resist machining forces. Two different geometric configurations of circular concave (Test 1-2) and convex (Test 3-4) components are considered in this study with its dimensions summarized in Table 5. The other cutting conditions such as *RDOC*, *ADOC*, workpiece geometry, cutting tool parameters etc. are maintained at constant level and tabulated in Table 5.

Table 5. Workpiece Dimension and Cutting Condition with varying Curvature.

Test No.	Geometry	Inner Radius (mm)	Outer Radius (mm)	Engagement Angle (θ_{en})
1.	Concave	35	41	66.77°
2.		55	61	63.82°
3.	Convex	39	45	55.86°
4.		59	65	57.08°

RDOC (mm)	:	4
ADOC (mm)	:	18
Workpiece Dimension (mm)	:	100 x 50 x 6 (L x H x D)
Final Thickness (mm)	:	2
Feed Rate (mm/min)	:	300
Spindle Speed (RPM)	:	2000

Figure 9(a) represents the cutting force variation obtained computationally for two different concave geometries at cutting conditions listed in Table 5 (Test 1 and 2). The cutting force decreases with the increase in radius of curvature owing to change of the engagement angle. Figure 9(b) shows the surface error variation determined computationally and experimentally for both concave geometries with higher (Test 2) and lower (Test 1) radius of curvature. It has been observed that the component with higher radius of curvature exhibits more surface error. This is primarily due to decrease in the stiffness of the concave geometries with increase in the radius of curvature. It has also been observed that the axial location of '*kink*' changes with change in workpiece radius of curvature. The axial location of '*kink*' in case of concave geometries moves upward due to decrease in the engagement angle which indicates delayed entry of the subsequent cutting flute in the cut.

Figure 10(a) represents the cutting force variation obtained computationally for two different convex geometries at cutting conditions listed in Table 5 (Test 3 and 4). The increase of cutting force with increase in radius of curvature can be attributed to change of the engagement angle. Figure 10(b) shows comparison of surface error variation predicted computationally and experimentally for both convex geometries with higher (Test 4) and lower (Test 3) radius of curvature. It can be seen that the component with higher workpiece curvature exhibits more surface error. Such behaviour can be attributed to two factors; (i) the increased engagement area leading to increased cutting forces on the component, and (ii) decrease in component stiffness with increase of workpiece curvature. It has also been realized that the axial location of '*kink*' changes with the change of workpiece curvature. The axial location of '*kink*' in case of convex geometries moves downward with increase of curvature due to increase in the engagement angle which signifies early entry of subsequent cutting flute into the cutting zone. However, small deviation between predicted and measured result is seen which may be due to various other factors such as vibrations, thermal effects, etc. which is neglected in the present study. The

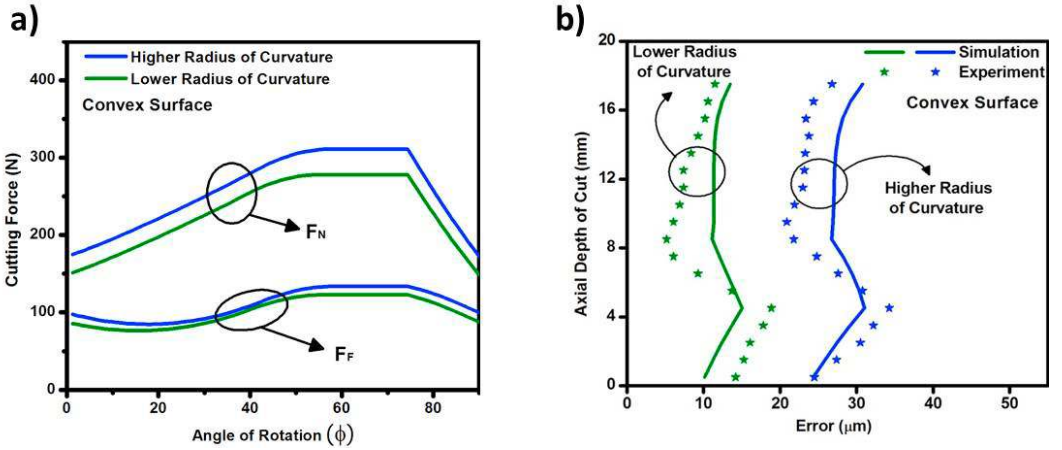

Fig. 10. End Milling of Convex Surface with varying Radius of Curvature: (a) Cutting Force Profile; (b) Surface Error Profile

subsequent studies can incorporate these aspects in the computational models to investigate the effects on the surface error.

4. Conclusions

This paper presented a comparison of axial variation of surface error during end milling of straight and circular concave and convex thin-walled components. The different aspects involved with the milling curved geometries such as effect of engagement area and radius of curvature have been investigated computationally and validated further by performing experiments. Based on outcomes of the present study, it has been realized that circular components deflects significantly lesser in comparison to straight components under identical cutting conditions despite the fact that concave geometries experience higher chip load and cutting forces. This is attributed to increase in the stiffness of circular component in comparison to straight geometries. To examine the effect of change in engagement area, the concept of '*Equivalent RDOC*' has been developed that offers constant engagement area by varying *RDOC* values for different geometries. It has been concluded that the convex geometries provide machining advantage allowing more productive cutting conditions without compromising surface error. It has been observed that the workpiece curvature influences both magnitude and profile of the surface error. The magnitude of surface error increases with workpiece curvature due to reduction in the stiffness of the curved components. Also the location of '*kink*' varies due to change in the engagement area of the cutting zone. The outcomes of the present study can be used effectively by process planners in selection of appropriate cutting conditions and devising machining strategies while designing roughing operation for thin-walled geometries.

Acknowledgements

The authors thank DST - Science and Engineering Research Board (SERB) (Project No.: YSS/2015/000495) and Ministry of Human Resource Development (MHRD), India for providing financial support to carry out this research work.

References

[1] Bera, T. C., Desai, K. A., Rao, P. V. M., 2010. On milling of thin-walled tubular geometries. Proceedings of the Institution of Mechanical Engineers, Part B: Journal of Engineering Manufacture, 224(12), 1804-1816.
[2] Sabberwal, A. J. P., Koenigsberger, F., 1961. Chip section and cutting force during the milling operation. Annals of the CIRP, 10(3), 197-203.
[3] Sutherland, J. W., Devor, R., 1986. An improved method for cutting force and surface error prediction in flexible end milling systems.Journal of Engineering for Industry, 108(4), 269-279.
[4] Ko, J. H., Yun, W. S., Cho, D. W., Ehmann, K. F., 2002. Development of a virtual machining system, part 1: approximation of the size effect for cutting force prediction. International Journal of Machine Tools and Manufacture, 42(15), 1595-1605.
[5] Zhang, L., Zheng, L., Zhang, Z. H., Liu, Y., Li, Z. Z., 2002. On cutting forces in peripheral milling of curved surfaces. Proceedings of the Institution of Mechanical Engineers, Part B: Journal of Engineering Manufacture, 216(10), 1385-1398.
[6] Zhang, L., Zheng, L., 2004. Prediction of cutting forces in milling of circular corner profiles. International Journal of Machine Tools and Manufacture, 44(2-3), 225-235.
[7] Rao, V. S., Rao, P. V. M., 2005. Modelling of tooth trajectory and process geometry in peripheral milling of curved surfaces. International Journal of Machine Tools and Manufacture, 45(6), 617-630.
[8] Desai, K. A., Agarwal, P. K., Rao, P. V. M., 2009. Process geometry modeling with cutter runout for milling of curved surfaces. International Journal of Machine Tools and Manufacture, 49(12-13), 1015-1028.
[9] Hao H, Wang B, Tang W., 2015. Prediction of instantaneous milling force taking runout into account in peripheral milling of curved surface. The International Journal of Advanced Manufacturing Technology, 79(1-4), 49-56.
[10] Kline, W. A., DeVor, R. E., Lindberg, J. R., 1982. The prediction of cutting forces in end milling with application to cornering cuts. International Journal of Machine Tool Design and Research, 22(1), 7-22.

[11] Yun, W. S., Ko, J. H., Cho, D. W., Ehmann, K. F., 2002. Development of a virtual machining system, part 2: prediction and analysis of a machined surface error. International Journal of machine tools and Manufacture, 42(15), 1607-1615.
[12] Budak, E., Altintas, Y., 1995. Modeling and avoidance of static form errors in peripheral milling of plates. International Journal of Machine Tools and Manufacture, 35(3), 459-476.
[13] Wan, M., Zhang, W., Qiu, K., Gao, T., Yang, Y., 2005. Numerical prediction of static form errors in peripheral milling of thin-walled workpieces with irregular meshes. J. Manuf. Sci. Eng., 127(1), 13-22.
[14] Ratchev, S., Liu, S., Huang, W., Becker, A. A., 2004. Milling error prediction and compensation in machining of low-rigidity parts. International Journal of Machine Tools and Manufacture, 44(15), 1629-1641.
[15] Rao, V. S., Rao, P. V. M., 2006. Effect of workpiece curvature on cutting forces and surface error in peripheral milling. Proceedings of the Institution of Mechanical Engineers, Part B: Journal of Engineering Manufacture, 220(9), 1399-1407.
[16] Dépincé, P., Hascoët, J.Y., 2006. Active integration of tool deflection effects in end milling. Part 2. Compensation of tool deflection. International Journal of Machine Tools and Manufacture, 46(9), 945-956.
[17] Schmitz, T. L., Couey, J., Marsh, E., Mauntler, N., Hughes, D., 2007. Runout effects in milling: Surface finish, surface location error, and stability. International Journal of Machine Tools and Manufacture, 47(5), 841-851.
[18] Bera, T. C., Desai, K. A., Rao, P. V. M., 2011. Error compensation in flexible end milling of tubular geometries. Journal of Materials Processing Technology, 211(1), 24-34.
[19] Desai, K. A., Rao, P. V. M., 2012. On cutter deflection surface errors in peripheral milling. Journal of Materials Processing Technology, 212(11), 2443-2454.
[20] Desai, K. A., Rao, P. V. M., 2016. Machining of curved geometries with constant engagement tool paths. Proceedings of the Institution of Mechanical Engineers, Part B: Journal of Engineering Manufacture, 230(1), 53-65.
[21] Bolar, G., Joshi, S. N., 2017. Three-dimensional numerical modeling, simulation and experimental validation of milling of a thin-wall component. Proceedings of the Institution of Mechanical Engineers, Part B: Journal of Engineering Manufacture, 231(5), 792-804.
[22] Arora, N., Agarwal, A., Desai, K. A., 2019. Modelling of static surface error in end-milling of thin-walled geometries. International Journal of Precision Technology, 8(2-4), 107-123.
[23] Wimmer, S., Hunyadi, P., Zaeh, M. F., 2019. A numerical approach for the prediction of static surface errors in the peripheral milling of thin-walled structures. Production Engineering, 13(3-4), 479-488.
[24] Wang, J., Ibaraki, S., Matsubara, A., 2017. A cutting sequence optimization algorithm to reduce the workpiece deformation in thin-wall machining. Precision Engineering, 50, 506-514.
[25] Li, Z. L., Zhu, L. M., 2019. Compensation of deformation errors in five-axis flank milling of thin-walled parts via tool path optimization. Precision Engineering, 55, 77-87.